Received: 1 March 2018 | Revised: 22 March 2019 | Accepted: 29 March 2019
DOI: 10.1111/exsy.12417

SPECIAL ISSUE PAPER

WILEY Expert Systems

Analysis and prediction of high-speed train wheel wear based on SIMPACK and backpropagation neural networks

Shuwen Wang[1] | Hao Yan[1] | Caixia Liu[1] | Ning Fan[1] | Xiaoming Liu[2] | Chengguo Wang[3]

[1] College of Mechanical Engineering, University of Shanghai for Science and Technology, Shanghai, China
[2] Institute of Mechanics, China Academy of Science, Beijing, China
[3] Research Center, China Academy of Railway Sciences, Beijing, China

Correspondence
Shuwen Wang, College of Mechanical Engineering, University of Shanghai for Science and Technology, Shanghai 200093, China.
Email: shuwenwang66@163.com

Funding information
National Natural Science Foundation of China (NSFC), Grant/Award Number: 51275126

Abstract

As train running speeds increase, the wheel–rail interactions of high-speed trains are becoming more complicated, and predicting and monitoring wheel wear are becoming increasingly important for the safe operation of high-speed trains. Therefore, identifying the critical factors that affect the wear of wheel–rail interactions and developing novel methods to predict wheel wear are of great importance. In this work, SIMPACK is used to establish a dynamic model of a high-speed train and to investigate the normal and lateral contact forces of the wheel–rail interfaces and the wear of the wheels for a train passing through a specially designed route that consists of straight-line, smooth-curved, and circular tracks. The wheel wear is predicted by means of the Archard wear model based on the SIMPACK analysis, and the wear is validated by a backpropagation neural network (BPNN) classification based on daily measured data provided by the Beijing Railway Administration. The results from the SIMPACK dynamic simulation and the BPNN classification show that the position of a wheel in a bogie has a significant effect on the wheel wear, but the position of a carriage in a train does not have a significant effect on the wheel wear. The findings from this study are very useful for the maintenance and safe operation of high-speed trains.

KEYWORDS

BP neural networks, high-speed train, SIMPACK, wheel wear

1 | INTRODUCTION

Many factors affect wheel–rail interactions and wear, such as the wheel and rail profiles, running speed, normal load, wheel material, suspension system, and operation environment. The effect of the rail roll angle on the contact condition was investigated in Bezin, Iwnicki, and Cavalletti (2008) and Zhai et al. (2014), and rail profile grinding may be an effective way to reduce rail wear and prolong rail service life (Alarcón, Burgelman, Meza, Toro, & Li, 2016). Because wheel–rail contact dynamics are too complicated to be simulated by laboratory test facilities, it is necessary and very important to develop theoretical models to study the factors affecting wheel–rail interactions and wear (Jin, Xiao, Wen, Guo, & Zhu, 2008). In recent decades, various finite element models have been developed and applied to wheel–rail steady-state rolling contact analyses (Chang, Wang, Chen, & Li, 2010) to predict the amount of material that is removed due to wheel–rail interactions (Ignesti, Malvezzi, Marini, Melia, & Rindia, 2012) and to analyse the effects of the normal load, punch angle, lateral displacement, and friction coefficient on the wheel–rail contact characteristics (Santamaría, Vadillo, & Oyarzabal, 2009; Xiao, 2012). SIMPACK, which was developed by INTEC Gmbh, is a well-known multibody simulation software that has been used by a number of researchers to study wheel–rail interactions (Ignesti, Malvezzi, Marini, Melia, & Rindia, 2012; Kurzeck, 2011; Molatefi, Hecht, & Bokaeian, 2017).

The simulation results in Tao, Wen, Zhao, and Jin (2016) show that, when considering a compromise between the calculation efficiency and accuracy of a wheel wear simulation, it may be a good choice to use the Hertz theory and FASTSIM (fast simulation) technique to solve the normal and tangential contact problems, respectively. However, analytical calculations of stresses based on the Hertz theory can only be applied to the elastic deformation of materials (Kuminek & Aniolek, 2014; Rovira, Roda, Marshall, Brunskill, & Lewis, 2011). A three-dimensional non-linear finite element dynamic analysis model was developed for the simulation of the wheel/rail rolling contact process, and the Archard wear model was applied with a cubic spline interpolation algorithm to obtain the wear distribution and the updated wheel/rail profiles (Chang, Wang, & Jin, 2010). Aceituno, Wang, Wang, and Shabana (2017) developed a wheel/rail wear prediction model integrated with a computational manual block system algorithm to study the effect of rail flexibility on wear prediction.

Simulating the form change of wheel–rail contacts helps to identify the risk of severe or catastrophic wear resulting from increased train speeds and axle loads and can help make more efficient maintenance plans for track and rolling stock (Telliskivi & Olofsson, 2004). Therefore, it is important to use a damage index model in multibody simulation software to predict the probability of rolling contact fatigue while suppressing the effects of wear for different friction control values (Khan, Persson, Lundberg, & Stenström, 2017). To study corrugation growth, a combination of models for short-term dynamic vehicle-track interactions and long-term damage is required (Torstensson, Pieringer, & Nielsen, 2014). Jin, Ishida, and Namura (2011) established a wear prediction model of the rail profile considering the contact stress, contact patch slip ratio, and material hardness based on the experimental results. However, the results of these contact models are usually postprocessed to estimate the wear on the profiles, and some of the hypotheses assumed in these contact models may be inadequate for wheel–rail wear analyses (Zhang, Li, Chu, Zu, & Wang, 2013).

Since 2002, the U.S. Federal Railway Administration has paid great attention to the application of large railway data and has carried out a number of projects involving large databases, image processing, and machine learning (Baillargeon, 2017). In China, Wang, Chen, and Liu (2007) used rail wear data measured by a large wheel–rail test dynamometer as the target samples of a backpropagation neural network (BPNN) for the prediction of rail wear losses.

A literature review shows that a constant train running speed was considered (Gordana, Franklin, & Fletcher, 2011; Wang, 2008; Xie, 2005) in some studies on wheel and rail wear for trains in China and other countries. The present work aims to investigate the effects of the train running speed, running route, and wheel position on the normal and lateral contact forces of the wheel–rail interface and the wear of the wheels for a high-speed train based on SIMPACK modelling and simulation analysis. The wheel wear prediction using this methodology is then validated through the application of a machine learning technique, BPNN, based on a large volume of daily measured wheel wear data that were collected by railway operators; such predictions have significant importance for the safe operation and maintenance of high-speed trains.

2 | SIMPACK DYNAMIC MODEL OF A HIGH-SPEED TRAIN

To investigate the effects of train running speed, running route, and wheel position on the normal and lateral contact forces of the wheel–rail interface and the wear of the wheels for a CRH380BL type electric multiple unit (EMU) high-speed train, a simplified dynamic model was developed by means of SIMPACK, as shown in Figure 1. The simplified train model consists of the basic elements in SIMPACK, such as body, joint, constraint, and force elements. The CRH380BL EMU high-speed train has a total of 16 carriages, each carriage has two bogies (front and rear), and each bogie has two wheelsets. The developed SIMPACK model in this study consists of only one carriage from the CRH380BL EMU train, which includes one carriage, two bogie frames, four wheelsets, and the primary and secondary suspension systems in each bogie frame. In this SIMPACK model, it is assumed that the normal and lateral forces and the operational conditions of all carriages are the same, and the effects of a carriage on the wheel–rail dynamics of other carriages are negligible. These assumptions may cause some errors during the analysis of the wheel–rail interactions and wheel wear of a high-speed train using the developed one-carriage SIMPACK model, but the BPNN classifications of the wheel wear based on the wheel diameter data measured by railway operators have justified the above assumptions; therefore, the developed one-carriage SIMPACK model is reasonably good for this study.

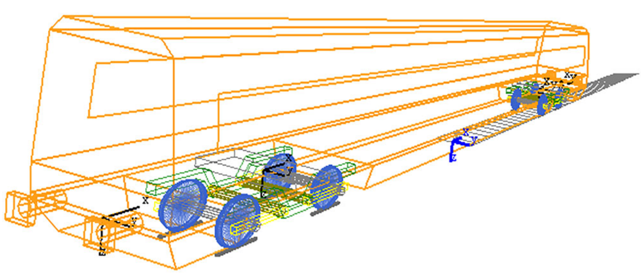

FIGURE 1 SIMPACK model of a CRH380BL electric multiple unit train carriage

The dynamic SIMPACK model parameters of the CRH380BL EMU train are shown in Table 1. The wheel tread of the CRH380BL EMU is LM_A (a standard wheel tread for high-speed trains in China), its matching track is CHN60, and the Hertz and FASTSIM methods (Tao, Wen, Zhao, & Jin, 2016) are used to calculate the normal and lateral forces in the wheel–rail interfaces, respectively.

As shown in Figure 2, when the lateral displacements are zero, the contact points between the wheels and rails are mainly on the top of the rails and the centres of the wheel treads. In this case, the contact stresses between the wheels and rails are the smallest, and the lateral creep rates/forces between the wheels and rails are very small. Figure 3 illustrates the forces applied on the outer and inner wheels when the train is running on a curved track.

Here, G is the total weight of a half axle and a wheel, $\alpha_{1,2}$ are the sharp angles between the normal contact forces and the gravitational forces (they are also called gravity angular stiffness), $F_{a1,2}$ are the centrifugal forces, $F_{n1,2}$ are the normal forces applied on the wheels, $F_{c1,2}$ are the lateral forces applied on the wheels, and $F_{f1,2}$ are the rolling frictional force generated by the wheels rolling on the rails. Subscripts 1 and 2 represent the outer and inner wheels, respectively. The driving torques applied on the wheels are not shown in Figure 3.

TABLE 1 SIMPACK model parameters of the CRH380BL EMU train

Parameter	Value	Unit
Train carriage mass	34,300	kg
Wheelset mass	1,713	kg
Wheel radius	0.46	m
Frame mass	2,439	kg
Rotational stiffness of primary series	54	MN/m
Lateral stiffness of primary series	5	MN/m
Vertical stiffness of primary series	0.95	MN/m
Rotational damping of primary series	52	MNs/m
Rotational stiffness of secondary series	0.131	MN/m
Lateral stiffness of secondary series	0.131	MN/m
Vertical stiffness of secondary series	0.261	MN/m
Rotational damping of secondary series	8.4	kNs/m

Abbreviation: EMU, electric multiple unit.

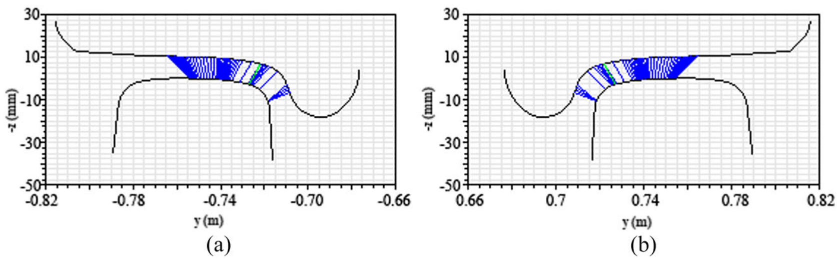

FIGURE 2 Contact interface between a wheel and rail: (a) outer wheel–rail contact and (b) inner wheel–rail contact

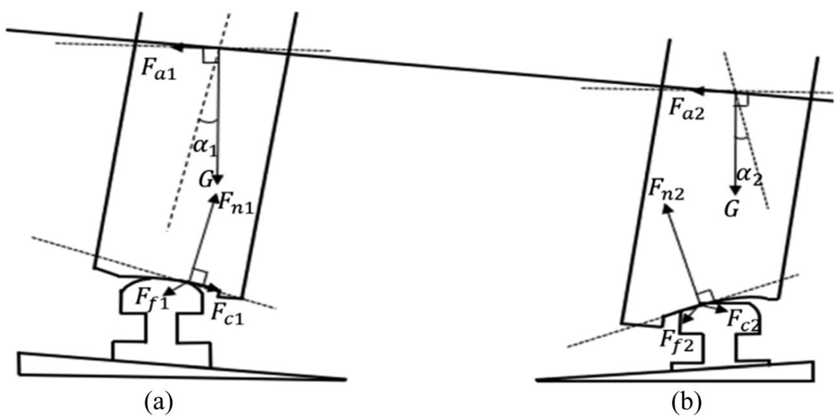

FIGURE 3 Illustration of the forces applied on the outer and inner wheels running on curved rails: (a) outer wheel–rail contact and (b) inner wheel–rail contact

3 | ANALYSIS OF THE FACTORS AFFECTING WHEEL WEAR BASED ON SIMPACK

In this study, the normal and lateral contact forces of the wheel–rail interface and the wear depths of the wheels will be analysed at different train running speeds based on the developed one-carriage SIMPACK model of the CRH380BL EMU train. The SIMPACK model is shown in Figure 1.

3.1 | Normal contact force of the wheel–rail interface

It is well known that the wear of a wheel and rail is proportional to the normal contact force (Gordana, Franklin, & Fletcher, 2011). The normal contact force of a wheel–rail interface is one of the most critical factors affecting the wear of a wheel and rail. In this study, the normal contact forces of the wheel–rail interface are calculated by means of the developed one-carriage SIMPACK model. Figures 4, 5, and 6 demonstrate the normal contact forces of the wheel–rail interface when the train is running on a specially designed operation route at speeds of 100, 200, and 300 km/hr, respectively. The specially designed train operation route is presented in Table 2.

Figures 4, 5, and 6 show that the normal contact forces of all wheels are the same, 57,500 N, when the train is running on the straight-line tracks at different operation speeds. However, the train operation speed and wheel position have significant effects on the normal contact forces of the wheel–rail interface when the train is running on circular and smooth-curved tracks due to the generated centrifugal forces. The centrifugal forces of the train increase as the operation speed increases when the train is running on curved and circular tracks.

Figure 4 shows that when the train is running on the designed tracks at a speed of 100 km/hr, the normal contact forces of the four left wheels (I, III, V, and VII) vary in the same way: (a) the normal contact forces remain constant on the first straight-line track, (b) decrease on the first

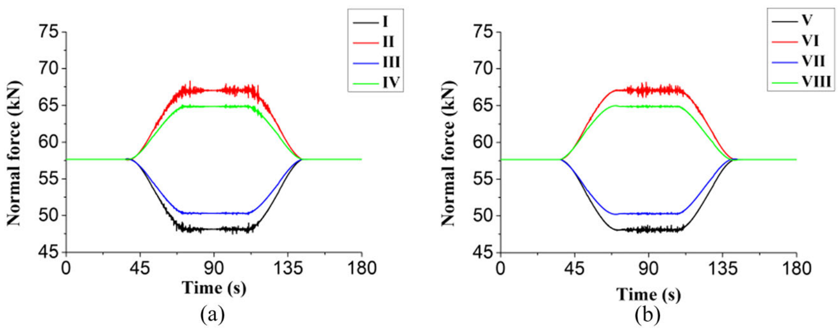

FIGURE 4 Normal contact forces of the wheel–rail interface at 100 km/hr: (a) Wheelsets 1 and 2 and (b) Wheelsets 3 and 4. I, left wheel of Wheelset 1; II, right wheel of Wheelset 1; III, left wheel of Wheelset 2; IV, right wheel of Wheelset 2. V, left wheel of Wheelset 3; VI, right wheel of Wheelset 3; VII, left wheel of Wheelset 4; VIII, right wheel of Wheelset 4

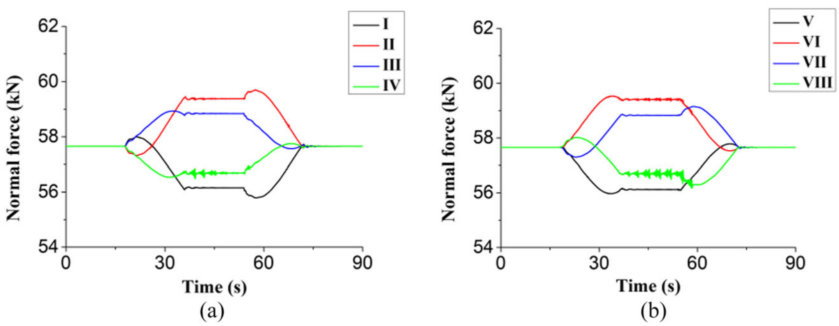

FIGURE 5 Normal contact forces of the wheel–rail interface at 200 km/hr: (a) Wheelsets 1 and 2 and (b) Wheelsets 3 and 4. I, left wheel of Wheelset 1; II, right wheel of Wheelset 1; III, left wheel of Wheelset 2; IV, right wheel of Wheelset 2; V, left wheel of Wheelset 3;VI, right wheel of Wheelset 3; VII, left wheel of Wheelset 4; VIII, right wheel of Wheelset 4

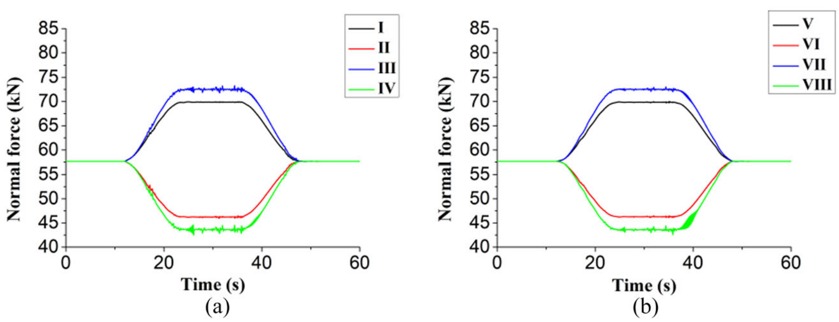

FIGURE 6 Normal contact forces of the wheel–rail interface at 300 km/hr: (a) Wheelsets 1 and 2 and (b) Wheelsets 3 and 4. I, left wheel of Wheelset 1; II, right wheel of Wheelset 1; III, left wheel of Wheelset 2; IV, right wheel of Wheelset 2. V, left wheel of Wheelset 3; VI, right wheel of Wheelset 3; VII, left wheel of Wheelset 4; VIII, right wheel of Wheelset 4

TABLE 2 Specially designed train operation route in the simulation

Operation track	Length (m)	Track radius (m)	Height (mm)
First straight-line track	1,000	0	0
First smooth-curved track	1,000	0–5,000	0–10
Circular track	1,000	5,000	10
Second smooth-curved track	1,000	5,000–0	10–0
Second straight-line track	1,000	0	0

smooth-curved track, (c) remain constant on the circular track, (d) increase on the second smooth-curved track, and (e) remain constant on the second straight-line track. The variations in the normal contact forces of the four right wheels (II, IV, VI, and VIII) are opposite to that of the four left wheels (I, III, V, and VII).

Figure 6 demonstrates that when the train is running on the smooth-curved and circular tracks at a speed of 300 km/hr, the gravity angular stiffness α_1 is decreased, and the gravity angular stiffness α_2 is increased. As a result, the normal contact forces of the four left wheels (I, III, V, and VII) exhibit the following trend as the train passes through the designed operation route: (a) the normal contact forces remain constant on the first straight-line track, (b) increase on the first smooth-curved track, (c) remain constant on the circular track, (d) decrease on the second smooth-curved track, and (e) remain constant on the second straight-line track. The variations in the normal contact forces of the four right wheels (II, IV, VI, and VIII) are opposite to that of the four left wheels (I, III, V, and VII).

However, when the train is running on the same designed operation route at a speed of 200 km/hr, the variations in the normal contact forces of the eight wheels are significantly different from those at speeds of 100 and 300 km/hr, as shown in Figure 5. In this case, the normal contact forces of Wheels I, IV, V, and VIII exhibit the following trend: (a) the normal contact forces remain constant on the first straight-line track, (b) decrease on the first smooth-curved track, (c) remain constant on the circular track, (d) increase on the second smooth-curved track, and (e) remain constant on the second straight-line track. The variations in the normal contact forces of Wheels II, III, VI, and VII are opposite to those of Wheels I, IV, V, and VIII.

3.2 | Lateral force

The lateral force has a significant effect on the normal contact stress between the wheel and rail, and an extremely large lateral force is responsible for train derailments. Figures 7, 8, and 9 show that when the train is running on the straight-line tracks, the lateral forces are zero. Figure 7 shows that when the train is travelling at a speed of 100 km/hr on the curved tracks, all wheelsets are subjected to positive lateral forces pointing to the outside of the curves. The lateral forces on Wheelsets 1 and 3 are approximately equal, and the maximum lateral force is 10,250 N on the circular track. Similarly, the lateral forces of Wheelsets 2 and 4 are equal, and the maximum lateral force is 1,744 N on the circular track.

Figure 8 shows that when the train is running at a speed of 200 km/hr, Wheelsets 1 and 3 are subjected to lateral forces pointing to the outside of the curves, whereas Wheelsets 2 and 4 are subjected to lateral forces pointing to the inside of the curves. The lateral forces of both Wheelsets 1 and 3 are 5,096 N on the circular track, and the lateral forces of both Wheelsets 2 and 4 are 4,236 N on the same circular track.

Figure 9 demonstrates that when the train is running at a faster speed of 300 km/hr, the centrifugal force is larger than the gravitational component of the train in the lateral direction. Then, all wheelsets are subjected to the lateral forces pointing to the inside of the curves. The lateral forces of Wheelsets 1 and 3 are equal, and their lateral forces are 4,952 N on the circular track. The lateral forces of Wheelsets 2 and 4 are equal, and their lateral forces are 12,554 N on the same circular track.

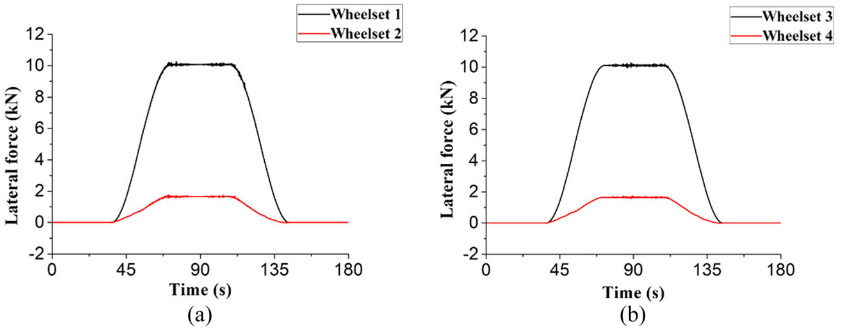

FIGURE 7 Lateral forces at 100 km/hr: (a) front bogie and (b) rear bogie

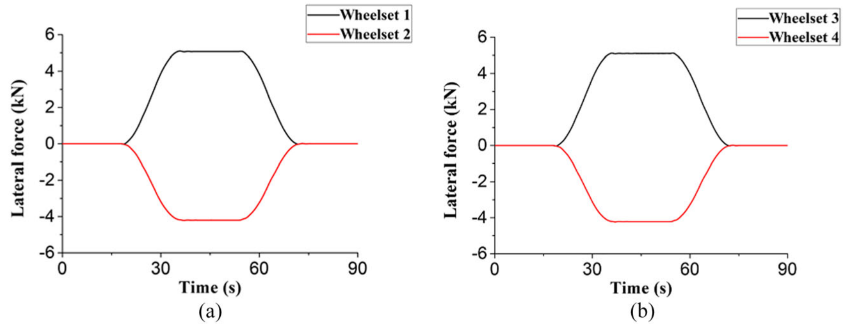

FIGURE 8 Lateral forces at 200 km/hr: (a) front bogie and (b) rear bogie

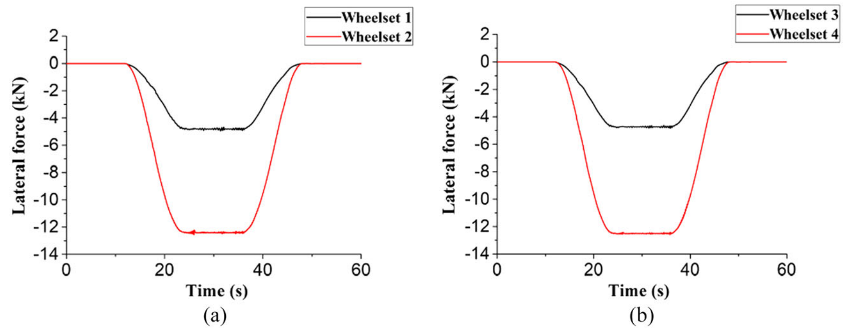

FIGURE 9 Lateral forces at 300 km/hr: (a) front bogie and (b) rear bogie

3.3 | Wheel wear prediction based on the Archard wear model

It is well known that the wear of wheels and rails is mainly caused by frictional energy generated on the wheel–rail interfaces in the rolling–sliding contacts. In this study, the prediction of wheel–rail wear is based on the widely used Archard wear model (Aceituno, Wang, Wang, & Shabana, 2017; Chang, Wang, & Jin, 2010; Jin, Ishida, & Namura, 2011; Gordana, Franklin, & Fletcher, 2011), and the wear volume calculation is based on the following equation:

$$V_{\text{wear}} = k_w \frac{Nd}{H},$$

where V_{wear} is the wear volume of the worn material; k_w is the dimensionless wear coefficient; N is the normal wheel–rail contact force; d is the sliding distance; and H is the hardness of the worn material (the wheel in this case). The value of k_w was obtained by extensive experiments (Chang, Wang, Chen, & Li, 2010). For a slow sliding speed with slight abrasion, k_w is in the range of $(1–4) \times 10^{-4}$; for a sliding speed of 0.2–0.7 m/s with substantial abrasion, k_w is in the range of $(30–40) \times 10^{-4}$; and for a high sliding speed and low contact pressure, k_w is in the range of $(1–10) \times 10^{-4}$. In this study, k_w and H are set to 1×10^{-4} and 280 HB (950×10^6 N/m^2), respectively, in the wheel wear calculation; these values are appropriate considering that the operation speed of the CRH380BL EMU train is high, but its wheel–rail contact pressure is lower than that of heavy-haul trains, and the hardness of the wheels of high-speed trains in China is in the range of 260–320 HB.

Based on the SIMPACK simulation and the above Archard wear model, the wear depths of the wheels after a certain period of operation can be predicted. Figure 10a,b presents the wear depths of the wheels in the front and rear bogies of the studied carriage after 5 and 30 days of operation, respectively. Because the wear depths of Wheels I, II, III, and IV in the front bogie are the same as those of Wheels V, VI, VII, and VIII in the

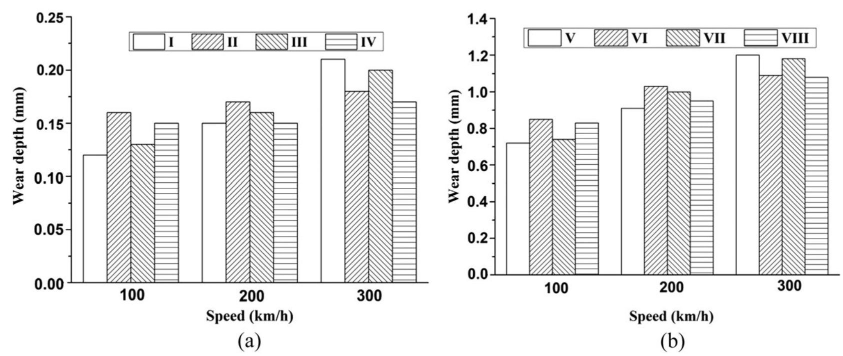

FIGURE 10 Wheel wear depths at different speeds: (a) 5 days and (b) 30 days. I, left wheel of Wheelset 1; II, right wheel of Wheelset 1; III, left wheel of Wheelset 2; IV, right wheel of Wheelset 2. V, left wheel of Wheelset 1; VI, right wheel of Wheelset 1; VII, left wheel of Wheelset 2; VIII, right wheel of Wheelset 2

rear bogie, respectively, only the wheel wear of the front bogie in the 5-day operation and the wheel wear of the rear bogie in the 30-day operation are illustrated as examples.

As shown in Figure 10a, when the train is running at speeds of 100 and 300 km/hr, the wear depths of the left wheels (I and III) are significantly different from those of right wheels (II and IV). The wear depths of Wheels I and III have no significant difference, and the wear depths of Wheels II and IV are also similar. The wear depths of Wheels I and III are less than those of Wheels II and IV when the train operation speed is 100 km/hr, but the wear depths of Wheels I and III are larger than those of Wheels II and IV when the train running speed is 300 km/hr. However, when the train running speed is 200 km/hr, the wear depths of the two diagonal wheels, I–IV and II–III, are similar. The wear depth of each wheel increases with increasing train operation period, as shown in Figure 10a,b.

4 | WHEEL WEAR PREDICTION BASED ON A BPNN

The wheel wear predicted in Section 3.3 is based on the well-known Archard wear model and the normal contact force simulated via the SIMPACK dynamic model. The accuracy of the wheel wear prediction and the effectiveness of the SIMPACK model must be validated before practical applications, which is the objective of data-driven model analysis based on BPNN.

The data that will be used in the BPNN identification or prediction are daily measured wheel wear depths or diameters of all the wheels of the 16-carriage CRH380BL EMU high-speed train over 30 continuous days of Beijing-Shanghai-Beijing daily operations. All data were measured by rail operators from the Beijing Railway Bureau. The train consists of 16 carriages, and each carriage has eight wheels. Therefore, there is a total of 3,840 (30 × 16 × 8) field-measured data used in the BPNN identification.

4.1 | Methodology

BPNNs have been developed for more than 30 years (Rumelhart, Hinton, & Williams, 1986), and the advantages of BPNNs compared with other neural networks (e.g., the radial basis function neural network) may be summarized as follows: (a) non-linear mapping capability; (b) self-learning and adaptive ability; (c) ability to apply learning outcomes to new knowledge; and (d) fault tolerance ability. The main idea of the backpropagation algorithm is to propagate the error of the output layer backward layer by layer to indirectly calculate the hidden layer error. More details about the theory and operation of a BPNN can be found in references (MacKay, 1992; Werbos, 1990; Widrow & Lehr, 1990). Because a three-layer BPNN is sufficient for most engineering applications, in this study, a three-layer BPNN is used to process the daily measured data to classify the wear depths of all wheels of the high-speed train, and a schematic diagram of the BPNN is shown in Figure 11.

4.2 | Case study

To establish a neural network, the input data must be preprocessed. In this case, the input data are the wheel position (1–8) and carriage number (1–16). Because the output of the neural network pattern can only be identified as 0 and 1, the values of the measured wheel wear (diameter reduction) are defined as 0 or 1. The maximum measured wheel diameter reduction is 2.5 mm, the minimum measured wheel diameter reduction is 1 mm, and most measured wheel diameter reductions are in the range of 1.5 to 2 mm. The measured wheel wear (diameter reductions) is divided into seven levels, and each level is represented by a binary number as follows: the wear range of [1, 1.5) is represented by 0000001; [1.5, 1.6) is represented by 0000010; [1.6, 1.7) is represented by 0000100; [1.7, 1.8) is represented by 0001000; [1.8, 1.9) is represented by 0010000; [1.9, 2.3) is represented by 0100000; and [2.3, 2.6) is represented by 1000000.

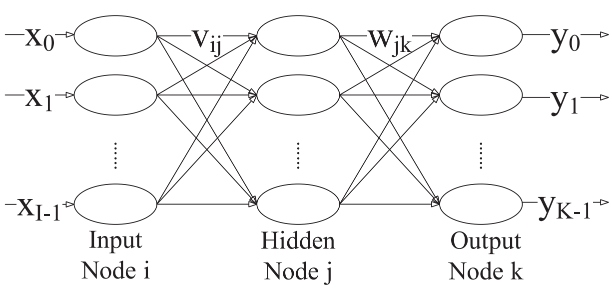

FIGURE 11 Schematic diagram of the three-layer backpropagation neural network

According to the empirical model (Xie, 2005), the following expression can be obtained:

$$S = \sqrt{0.43mn + 0.12n^2 + 2.54m + 0.77n + 0.35} + 0.51,$$

where m = 2 is the number of input nodes, n = 7 is the number of output nodes, and S is the number of hidden nodes, which is calculated as 5.

Before the BPNN operation, the well-known Sigmoid function is chosen as the neural network stimulus function, the initial value of the training learning rate is set to 0.1, the momentum coefficient is set to 0.95, and the maximum training time is set to 10000. When the system error is less than 0.01, it will be considered that the network is convergent. The percentage of training samples, validated samples, and test samples are designed to be 70%, 15%, and 15%, respectively.

After 31 training cycles, the network converged, and the mean square error was less than 0.009. At this time, the training sample, verification sample, and test sample recognition rate are 96.1%, 94.7%, and 100%, respectively, which satisfies the criteria outlined above. The threshold values of the input layer to the hidden layer are as follows:

$$\begin{bmatrix} 2.1413 & 0.6719 \\ 0.0047 & -8.298 \\ 0.123 & -8.4408 \\ -0.1749 & 6.994 \\ -0.0066 & -6.4992 \end{bmatrix}.$$

The hidden layer threshold values are as follows:

$$[-3.9207 -1.2902\ 6.5262\ 6.9563\ 1.6081]^T.$$

The weights of the hidden layer to the output layer are as follows:

$$\begin{bmatrix} 2.7309 & 0.9073 & -2.2063 & -1.4267 & -1.7308 \\ 1.2589 & 1.9912 & -1.3258 & -1.6424 & -2.1964 \\ 1.2855 & 4.7701 & 2.0616 & 2.9132 & -5.1989 \\ -0.8498 & -3.0176 & -5.1678 & -3.5308 & 6.5662 \\ 0.5206 & -4.5689 & 0.4916 & -1.2959 & 2.1583 \\ 2.2635 & 1.846 & -0.843 & -1.1886 & -1.9047 \\ 0.0431 & 3.4984 & -0.2745 & 6.3082 & 0.8743 \end{bmatrix}.$$

The output layer threshold values are as follows:

$$[-1.7071 -1.5641 -1.628\ 2.5132 -2.5381 -0.2744\ 0.0864]^T.$$

Using the trained network above, the wheel wear (diameter reduction) of carriage No. 1 is classified as shown in Table 3. The identified diameter reductions of Wheels I, IV, V, and VIII in carriage No. 1 are [1.7, 1.8), which are smaller than those of the diameter reductions of Wheels II, III, VI, and VII in the same carriage of [1.8, 1.9). This indicates that the position of the wheel has a significant effect on the wheel wear, which is consistent with the results predicted using the SIMPACK model when the train operation speed is 200 km/hr, as shown in Figure 10. The identified wear by means of the BPNN are the diameter reductions of Wheels I through VIII, whereas the predicted wear of the wheels shown in Figure 10 are the wear depths (half of the wheel diameter reductions) of Wheels I to VIII.

TABLE 3 Wheel wear prediction results of carriage No. 1

Wheel position	Prediction result code	Wear range (wheel diameter reduction)
1	0001000	[1.7, 1.8)
2	0010000	[1.8, 1.9)
3	0010000	[1.8, 1.9)
4	0001000	[1.7, 1.8)
5	0001000	[1.7, 1.8)
6	0010000	[1.8, 1.9)
7	0010000	[1.8, 1.9)
8	0001000	[1.7, 1.8)

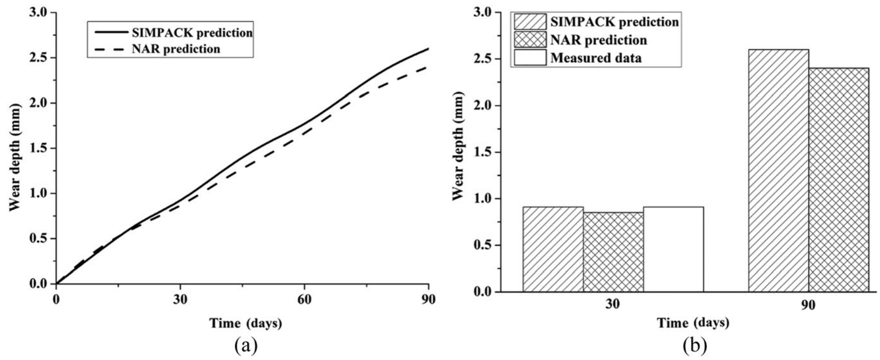

FIGURE 12 Wear depths of Wheel I: (a) NAR and SIMPACK predictions and (b) NAR/SIMPACK predictions and field-measured data. NAR, non-linear autoregressive

The wear (diameter reductions) of Wheel I in all 16 carriages has also been identified in the range of [1.7, 1.8) by means of the BPNN operation, indicating that the position of a carriage has no significant effect on the wear of wheels. This finding verified that the developed simplified one-carriage SIMPACK model can be effectively used to predict the wear of wheels of high-speed trains.

4.3 | Comparison between the non-linear autoregressive prediction and SIMPACK simulation

To predict the wheel wear over a longer period of train operation, the non-linear autoregressive (NAR) model is employed. In comparison, the wear depths of Wheel I after 90 days of operation are predicted by means of the NAR and SIMPACK models, as shown in Figure 12a. The field-measured data are from the CRH380BL EMU high-speed train between Beijing and Shanghai. The distance between Beijing and Shanghai is 1,250 km, and it takes approximately 6 hr to travel from Beijing to Shanghai via the high-speed train. The average speed of the high-speed train is approximately 208 km/hr. Therefore, a train operation speed of 200 km/hr is used in the SIMPACK wear prediction, and it is compared with the field measured and the NAR-predicted wear depths in Figure 12b. It can be seen from Figure 12 that the predicted wear depths of Wheel I from the NAR and SIMPACK models agree well with the field-measured data, which validated the NAR and SIMPACK models.

5 | CONCLUSIONS

In this study, wheel wear is simulated by a SIMPACK dynamic analysis and classified by BPNNs. In the SIMPACK dynamic analysis, the effects of the train running speed, operation route, and wheel position on the normal and lateral contact forces of the wheel–rail interface and the wear of the wheels were investigated. Based on daily measured data, the BPNN was employed to classify the wear of each wheel of the high-speed train, which validated the simplified SIMPACK model of the high-speed train and may provide guidance for the maintenance and safe operation of high-speed trains. The following conclusions may be obtained:

- Based on the SIMPACK analysis, the operation speed of a high-speed train has a significant effect on the normal and lateral contact forces of a wheel–rail interface when the train is running on curved and circular tracks.
- The position of a bogie in the train does not have a significant effect on the wear of the wheels, but the position of a wheel in a bogie has a significant effect on the wear of the wheel; this conclusion can be obtained from both the SIMPACK analysis based on the Archard model and the BPNN classification. The developed one-carriage SIMPACK model of a high-speed train can be effectively used to simulate the normal and lateral contact forces of a wheel–rail interface and the wear of the wheels for a high-speed train.
- Based on the daily measured data of wheel diameters, a NAR can be effectively used to predict the wear of each wheel of a high-speed train, which is very useful for the maintenance of train wheels and the safe operation of high-speed trains.

ORCID

Shuwen Wang https://orcid.org/0000-0003-3147-7648

REFERENCES

Aceituno, J. F., Wang, P., Wang, L., & Shabana, A. A. (2017). Influence of rail flexibility in a wheel/rail wear prediction model. *Proceedings of the Institution of Mechanical Engineers Part F Journal of Rail & Rapid Transit*, *231*, 57–74. https://doi.org/10.1177/0954409715618426

Alarcón, G. I., Burgelman, N., Meza, J. M., Toro, A., & Li, Z. (2016). Power dissipation modelling in wheel/rail contact: Effect of friction coefficient and profile quality. *Wear*, *366-367*, 217–224. https://doi.org/10.1016/j.wear.2016.04.026

Baillargeon, J. P. (2017). Safe transportation powered by big data. Newark: Fourth Annual Conference on Big Data.

Bezin, Y., Iwnicki, S. D., & Cavalletti, M. (2008). The effect of dynamic rail roll on the wheel–rail contact conditions. *Vehicle System Dynamics*, *46*(sup1), 107–117. https://doi.org/10.1080/00423110701882348

Chang, C., Wang, C., Chen, B., & Li, L. (2010). A study of a numerical analysis method for the wheel–rail wear of a heavy-haul train. *Proceedings of the Institution of Mechanical Engineers Part F Journal of Rail & Rapid Transit*, *224*, 73–482. https://doi.org/10.1243/09544097JRRT341

Chang, C., Wang, C., & Jin, Y. (2010). Study on numerical method to predict wheel/rail profile evolution due to wear. *Wear*, *269*, 167–173. https://doi.org/10.1016/j.wear.2009.12.031

Gordana, V., Franklin, F., & Fletcher, D. (2011). Influence of partial slip and direction of traction on wear rate in wheel–rail contact. *Wear*, *270*, 163–171. https://doi.org/10.1016/j.wear.2010.10.012

Ignesti, M., Malvezzi, M., Marini, L., Melia, E., & Rindia, A. (2012). Development of a wear model for the prediction of wheel and rail profile evolution in railway systems. *Wear*, *284*, 1–17. https://doi.org/10.1117/12.509378

Jin, X., Xiao, X., Wen, Z., Guo, J., & Zhu, M. (2008). An investigation into the effect of train curving on wear and contact stresses of wheel and rail. *Tribology International*, *42*, 475–490. https://doi.org/10.1016/j.triboint.2008.08.004

Jin, Y., Ishida, M., & Namura, A. (2011). Experimental simulation and prediction of wear of wheel flange and rail gauge corner. *Wear*, *271*, 259–267. https://doi.org/10.1016/j.wear.2010.10.032

Khan, S. A., Persson, I., Lundberg, J., & Stenström, C. (2017). Prediction of top-of-rail friction control effects on rail RCF suppressed by wear. *Wear*, *380-381*, 106–114. https://doi.org/10.1016/j.wear.2017.03.010

Kuminek, T., & Aniolek, K. (2014). Methodology and verification of calculations for contact stresses in a wheel–rail system. *Vehicle System Dynamics*, *52*, 111–124. https://doi.org/10.1080/00423114.2013.863361

Kurzeck, B. (2011). Combined friction induced oscillations of wheelset and track during the curving of metros and their influence on corrugation. *Wear*, *271*, 299–310. https://doi.org/10.1016/j.wear.2010.10.049

MacKay, D. J. C. (1992). A practical Bayesian framework for backpropagation networks. *Neural Computation*, *4*, 448–472. https://doi.org/10.1162/neco.1992.4.3.448

Molatefi, H., Hecht, M., & Bokaeian, V. (2017). Stability and safety analysis of an active steering bogie according to EN 14363 standard. *Journal of the Brazilian Society of Mechanical Sciences & Engineering*, *39*, 2945–2956. https://doi.org/10.1007/s40430-017-0758-0

Rovira, A., Roda, A., Marshall, M. B., Brunskill, H., & Lewis, R. (2011). Experimental and numerical modelling of wheel–rail contact and wear. *Wear*, *271*, 911–924. https://doi.org/10.1016/j.wear.2011.03.024

Rumelhart, D. E., Hinton, G. E., & Williams, R. J. (1986). Learning representations by back-propagating errors. *Nature*, *323*(6088), 533–536. https://doi.org/10.1016/B978-1-4832-1446-1446-35-2

Santamaría, J., Vadillo, E. G., & Oyarzabal, O. (2009). Wheel–rail wear index prediction considering multiple contact patches. *Wear*, *267*, 1100–1104. https://doi.org/10.1016/j.wear.2008.12.040

Tao, G., Wen, Z., Zhao, X., & Jin, X. (2016). Effects of wheel–rail contact modelling on wheel wear simulation. *Wear*, *366-367*, 146–156. https://doi.org/10.1016/j.wear.2016.05.010

Telliskivi, T., & Olofsson, U. (2004). Wheel–rail wear simulation. *Wear*, *257*, 1145–1153. https://doi.org/10.1016/j.wear.2004.07.017

Torstensson, P. T., Pieringer, A., & Nielsen, J. (2014). Simulation of rail roughness growth on small radius curves using a non-Hertzian and non-steady wheel–rail contact model. *Wear*, *314*, 241–253. https://doi.org/10.1016/j.wear.2013.11.032

Wang, W. (2008). Study on coupling relation between wheel rail rolling contact fatigue and wear and preventive measures. PhD Dissertation, Southwest Jiaotong University.

Wang, W., Chen, M., & Liu, Q. (2007). *Prediction of rail wear based on BP neural network. Lubrication and seal* (Vol. 32) (pp. 20–22). https://doi.org/10.3969/j.issn.0254-0150.2007.12.006

Werbos, P. J. (1990). Backpropagation through time: What it is and how to do it. *Proceedings of IEEE*, *78*, 1550–1560. https://doi.org/10.1109/5.58337

Widrow, B., & Lehr, M. A. (1990). 30 years of adaptive neural networks: Perceptron, madaline, and backpropagation. *Proceedings of IEEE*, *78*, 1415–1442. https://doi.org/10.1109/5.58323

Xiao, Q. (2012). The elasto-plastic analysis and fatigue damage research of wheel–rail rolling contact. PhD Dissertation, China Academy of Railway Sciences.

Xie, X. (2005). Research on pattern recognition based on BP neural network in visual inspection system. Master's Thesis, Harbin University of Science and Technology. Doi:CNKI:CDMD: 2.2005.150830

Zhai, W., Gao, J., Liu, P., & Wang, K. (2014). Reducing rail side wear on heavy-haul railway curves based on wheel–rail dynamic interaction. *Vehicle System Dynamics*, *52*(sup1), 440–454. https://doi.org/10.1080/00423114.2014.906633

Zhang, Z., Li, G., Chu, G., Zu, H., & Wang, Y. (2013). Simulation analysis of the influence of wheel diameter difference on the dynamic performance of locomotive. *Railway Locomotive & CAR*, *33*(2), 11–15. https://doi.org/10.3969/j.issn.1008-7842.2013.02.04

AUTHOR BIOGRAPHIES

Shuwen Wang is a Professor in the College of Mechanical Engineering at the University of Shanghai for Science and Technology (USST), China. Professor Wang got his Master's degree from the University of Toronto in Canada and PhD from the Department of Engineering at the University of Cambridge in the United Kingdom. Professor Wang's current research interests are friction-induced vibration and noise control, structural dynamics, tribology, and surface engineering.

Hao Yan is a Master's degree Student at USST under the supervision of Prof. Shuwen Wang.

Caixia Liu is a Master's degree Student at USST under the supervision of Prof. Shuwen Wang.

Ning Fan was a Master's degree Student at USST under the supervision of Prof. Shuwen Wang.

Xiaoming Liu got his PhD from Tsinghua University and is working as an associate professor in the Institute of Mechanics, China Academy of Sciences. Dr. Liu's current research interests are computational mechanics and structural dynamics.

Chengguo Wang was a professor in the Research Center of China Academy of Railway Science, China. Prof. Chengguo Wang is the receiver of more than 20 scientific prizes from China Railway Society and China Railway Ministry including Mao Yisheng Prize of China Railway Technology. Prof. Wang has published more than 100 scientific papers including 5 best papers selected by the International Railway Society and 30 best papers selected by China Railway Society.

How to cite this article: Wang S, Yan H, Liu C, Fan N, Liu X, Wang C. Analysis and prediction of high-speed train wheel wear based on SIMPACK and backpropagation neural networks. *Expert Systems*. 2019;e12417. https://doi.org/10.1111/exsy.12417